

**Product Development Team
for
NEXRAD Enhancements**

Quarterly Report – 1st Quarter FY 03

03.6.2 Polarization and Frequency Diversity

Algorithms based on polarimetry will meet the aviation needs for information about the volumetric extent of hail, freezing rain, snow, and icing conditions, as well as non-hydrometeor scatterers. The biggest potential payoff is enhanced data quality. For all practical purposes, polarimetric techniques will eliminate problems associated with sea-clutter, ground clutter, AP, and biological scatterers.

a) Current Efforts

(NSSL):

An improved version of the classification algorithm based on the use of polarimetric data has been developed. A list of hydrometeor classes has been extended by adding frozen particles: dry snow and wet snow. Current version contains seven classes of radar echo: (1) ground clutter (anomalous propagation), (2) biological scatterers (insects and birds), (3) dry snow, (4) wet snow, (5) stratiform rain, (6) convective rain, and (7) rain/hail mixture.

Automatic real-time classification is made at two lowest elevation angles: 0.5 and 1.5°. Some elements of a pattern recognition methodology were added to the basic fuzzy logic scheme. For example, the algorithm checks for horizontal and vertical continuity of the class products, their consistency, etc. Results of classification are routinely delivered in real-time to operational office of National Weather Service in Norman and can be viewed at the web site <http://www.nssl.noaa.gov/~hondl/radar>.

Examples of radar data fields and results of classification are presented in Figs. 1 and 2.

All seven classes of radar echo are presented in the case of a summer mesoscale convective system in Fig. 1. It is important that the classification algorithm clearly delineates liquid and frozen hydrometeors at the 0.5° elevation conical scan. Thus, the height of the melting level (depending on the azimuth direction) can be easily determined. This capability allows us to assess the quality of rain-fall estimation from the data taken at the 0.5° elevation. Indeed, to the north of the radar, rain estimates become contaminated by the bright band and the presence of the frozen hydrometeors starting at ranges 130 - 140 km from the radar.

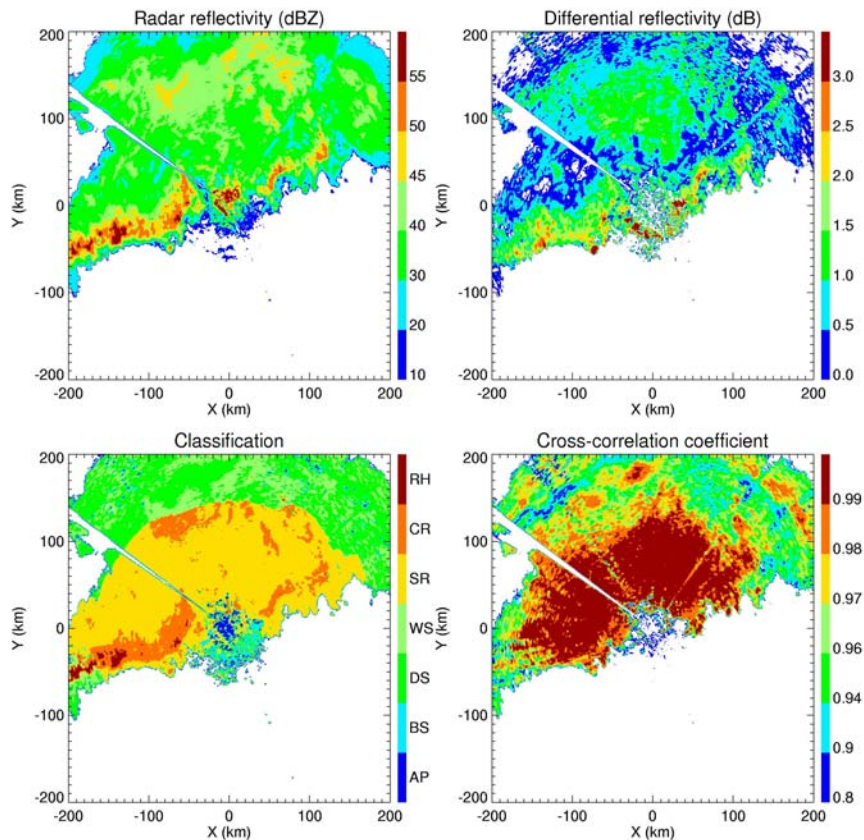


Figure 1. Fields of radar reflectivity Z , differential reflectivity Z_{DR} , cross-correlation coefficient ρ_{hv} , and results of classification for the MCS case on 06/16/02. Elevation angle is 0.5° , AP stands for anomalous propagation/ground clutter, BS for biological scatterers, DS for dry snow, WS for wet snow, SR for stratiform rain, CR for convective rain, and RH for rain/hail mixture.

The case presented in Fig. 2 illustrates discrimination between AP, biological scatterers (birds in this case), and rain. Here rain is characterized by high ρ_{hv} and moderately positive values of Z_{DR} , whereas the echoes from the ground and birds have very low ρ_{hv} and extreme values of Z_{DR} (negative for AP and high positive for birds). Notable are the areas of AP embedded in light rain to the east and south of the radar. Most likely, these AP echoes are caused by cold air outflow from the thunderstorms in the SE sector of the radar echo. Extensive clear-air BS echoes are associated with the Fall bird migration that rapidly intensified after convective storm swept across the observation area.

Detailed Cases

Data collected by the NSSL Polarimetric WSR-88D (KOUN) during a severe mesoscale convective system (MCS) on 15-16 June 2002 were studied (Fig. 3). A region of low signal-to-noise ratio, caused by attenuation due to heavy precipitation, was easily identified using the correlation coefficient field (Fig. 4).

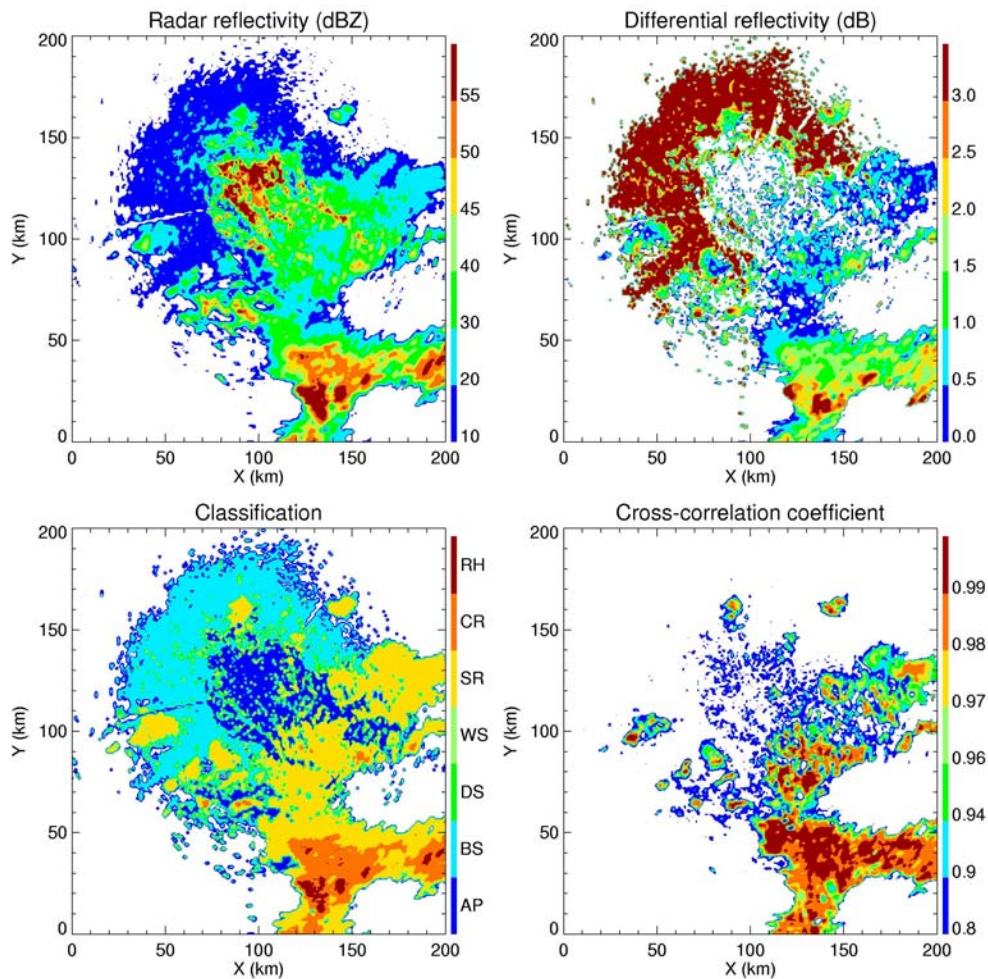


Figure 2. Same as in Fig. 2 but for the case of 10/06/02.

This is the first available KOUN case with such attenuation. The hydrometeor classification algorithm (HCA) identified a number of signatures consistent with hail. These data were used in real time warning operations at the National Weather Service (NWS) forecast office.

Data collected by KOUN during an outbreak of hail-producing severe thunderstorms on 18 September 2002 were also studied (Fig. 5). Well-defined local minima in differential reflectivity (Fig. 6) were found at low levels in several thunderstorms that produced very large hail at the surface. Frequently corresponding to these signatures were low correlation coefficient values (Fig. 7), another indicator of large hail. The HCA identified hail in several storms where hail was verified to be falling at ground level (Fig. 8). These data were also used in real time warning operations at the NWS forecast office. A case study document was prepared and distributed to NWS forecasters, illustrating the utility of polarimetric radar in identifying hail on 18 September.

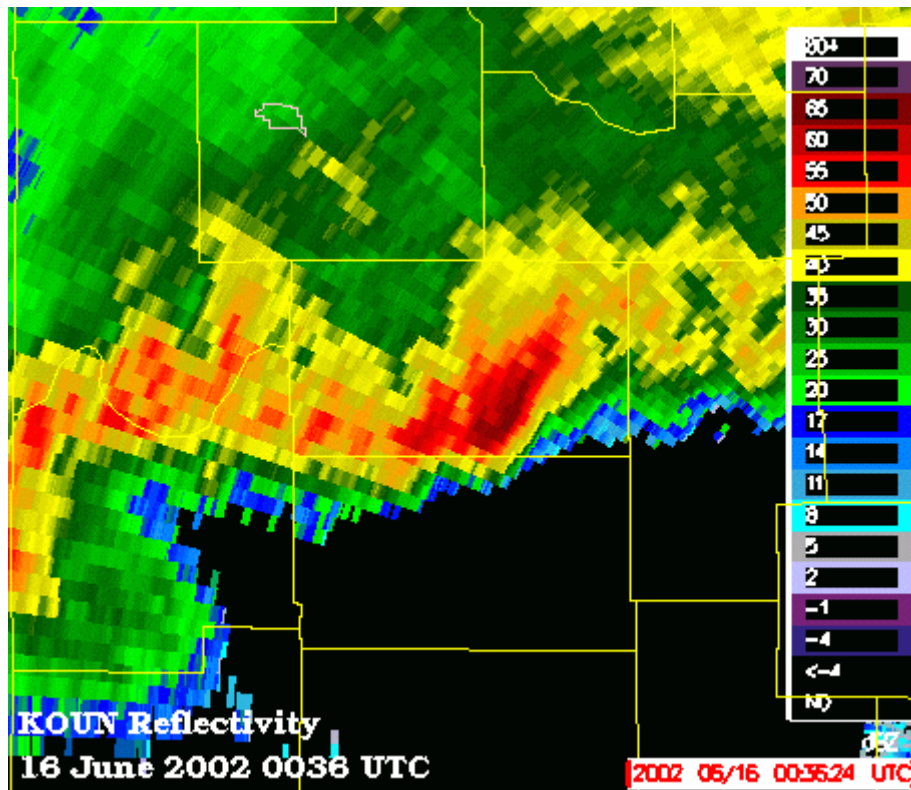


Figure 3. KOUN reflectivity at 16 June 2002 0036 UTC. View is toward the northwest at a severe hail-producing segment of a mesoscale convective system.

Analysis continued on research polarimetric data containing storms which producing damaging wet microbursts (Fig. 9). A layer of high specific differential phase shift (Fig. 10) is frequently noted below the reflectivity maximum, indicating a layer of water-coated, melting hailstones within the downdraft column. It is surmised these microbursts are driven by diabatic cooling provided by the phase change from hail to rain.

A case was analyzed (24 October 2002) in which a well-defined area of enhanced, non-precipitating echoes moved across the KOUN data collection area (Fig. 11). The HCA indicated the presence of birds and/or insects (Fig. 12). Although the presence of birds and/or insects cannot be independently confirmed, two rain gauges recorded no precipitation as the echoes passed overhead.

A new cold season version of the HCA was received 20 November 2002. Initial work began to re-run the HCA on archived cases. Also, local software display packages were updated to allow real time use and verification of the new HCA. In addition, several radar data sets of light rain events were collected by KOUN during November. These cases are being used to fine-tune the new HCA in discriminating light rain from snow when low signal-to-noise ratio echoes are dominant.

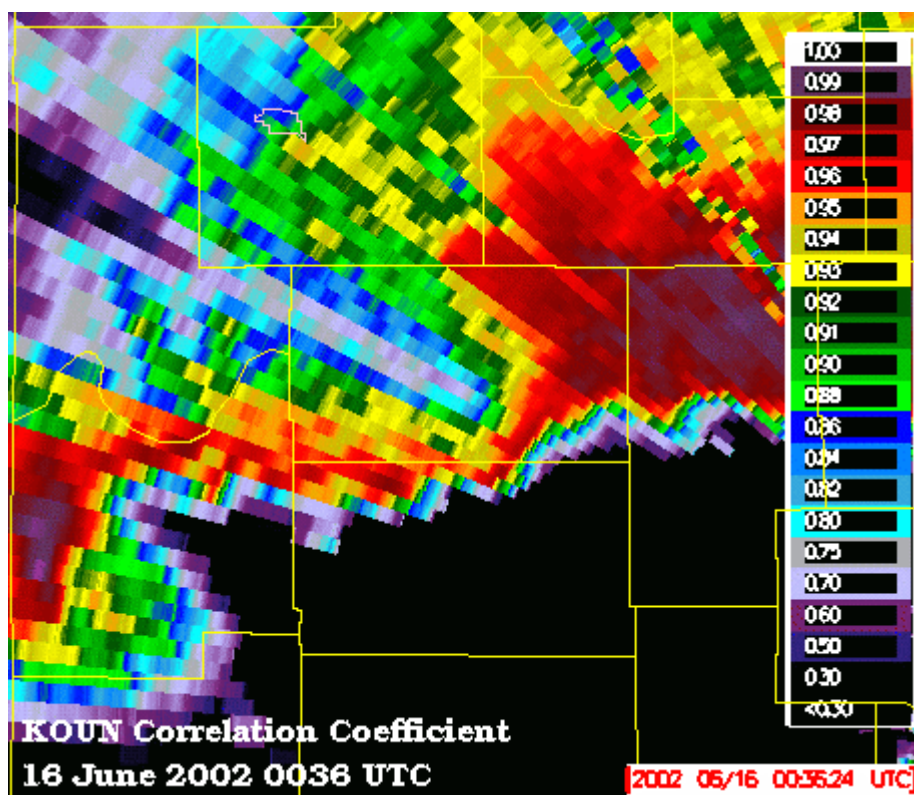


Figure 4. KOUN correlation coefficient at 16 June 2002 0036 UTC. View is toward the northwest. Severe beam attenuation that was not evident in the reflectivity is clearly seen where a “shadow” of low correlation coefficient is cast behind the core of heavy rain and hail.

Data were collected by KOUN during a winter storm on 3-5 December 2002. Snow was observed over northwestern Oklahoma, rain over central and southeastern Oklahoma, and a band of freezing rain fell between the snow and rain areas. These data were evaluated in real time at the NWS Forecast Office. Although a special sounding (Fig. 13) indicated a freezing level well above the rain/snow line detected by KOUN (Fig. 14), research indicates a 500-meter deep layer of partially-melted snow below the ambient freezing level is typical in sub-saturated environments. Therefore, the HCA output was found to be consistent with the sounding's temperature profile.

(NCAR):

TASK 03.6.2.10: Winter storm case studies

Unfortunately, drought conditions persist in the Boulder, CO, area. Video disdrometer data have been collected for only two brief snow events. Hence, progress concerning the distribution of ice particles in winter storms has been slow. This effort supports studies for improving the quantitative estimation of snowfall and provides verification for the hydrometeor classification algorithm.

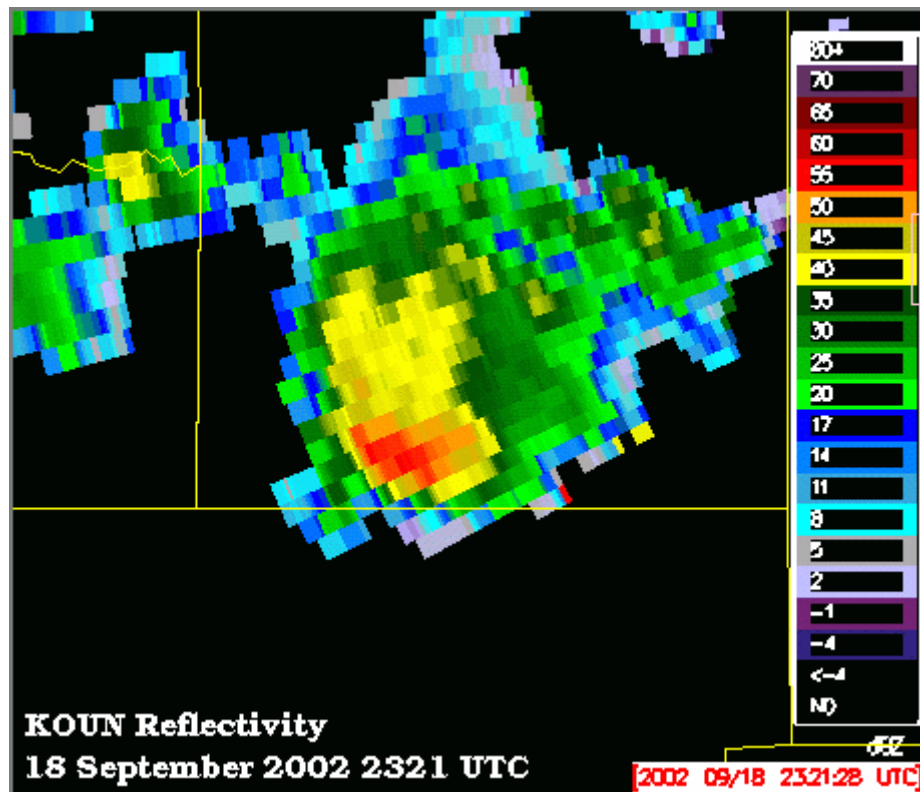


Figure 5. KOUN reflectivity at 18 September 2002 2321 UTC. View is toward the southwest at a hail-producing severe thunderstorm.

TASK 03.6.2.11: Implement improved hail detection algorithm

The upgrade to the hail detection algorithm for real time operation on NCAR's polarimetric radar is on hold until the budget picture is clarified.

TASK 03.6.2.12: Test NCAR freezing level algorithm

The freezing level algorithm was run on additional cases. Fig. 15 shows an analysis for an IMPROVE II event that occurred on 13 December 2001. Designations were made for a 5-km grid to the east of the radar using radar reflectivity, linear depolarization ratio, and co-polar correlation coefficient. Summary results are shown for the individual radar parameters and for the algorithm consensus estimate. Verification data from the National Weather Service sounding site at Salem, Oregon and from special sounding sites are also given. These sites are 40-80 km from the radar. Note that the algorithm appears to have captured detailed information regarding the temporal evolution of the freezing level. Two formal papers describing the algorithm and application are in preparation in fulfillment of 03.6.2.E12

b) Planned Efforts

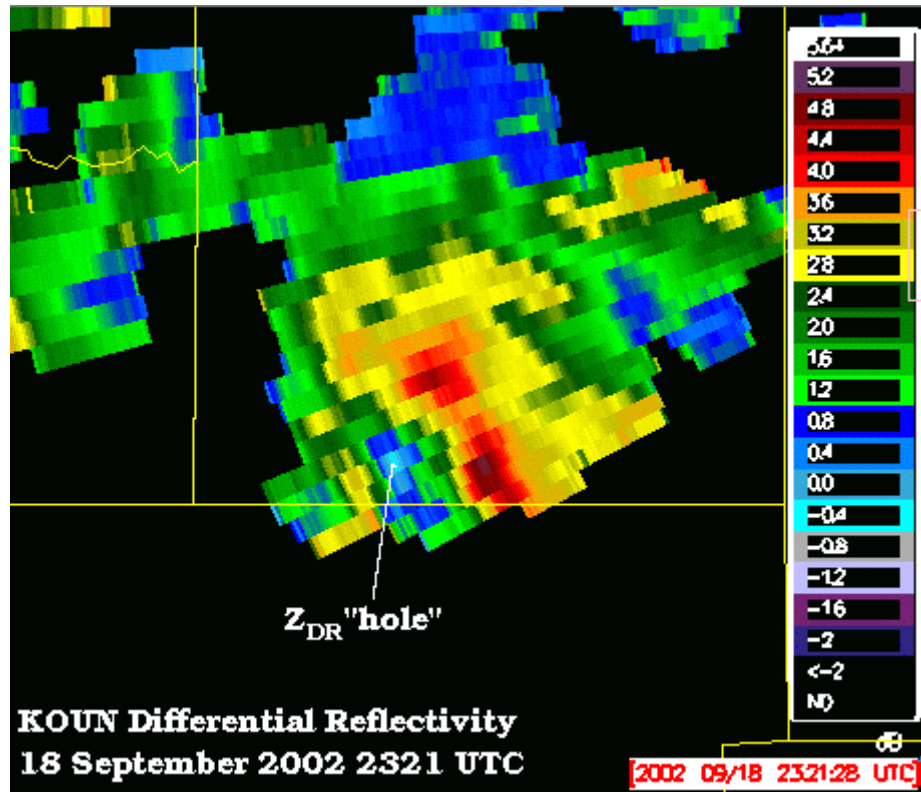


Figure 6. KOUN differential reflectivity (Z_{DR}) at 18 September 2002 2321 UTC. View is toward the southwest. A distinct “hole” in the Z_{DR} field is coincident with the region of maximum reflectivity in Fig. 5. Spotters near the location of the Z_{DR} hole reported damaging hail 4.5 inches in diameter.

c) Problems/Issues

None.

d) Interface with other Organizations

None.

e) Activity Schedule Changes

None.

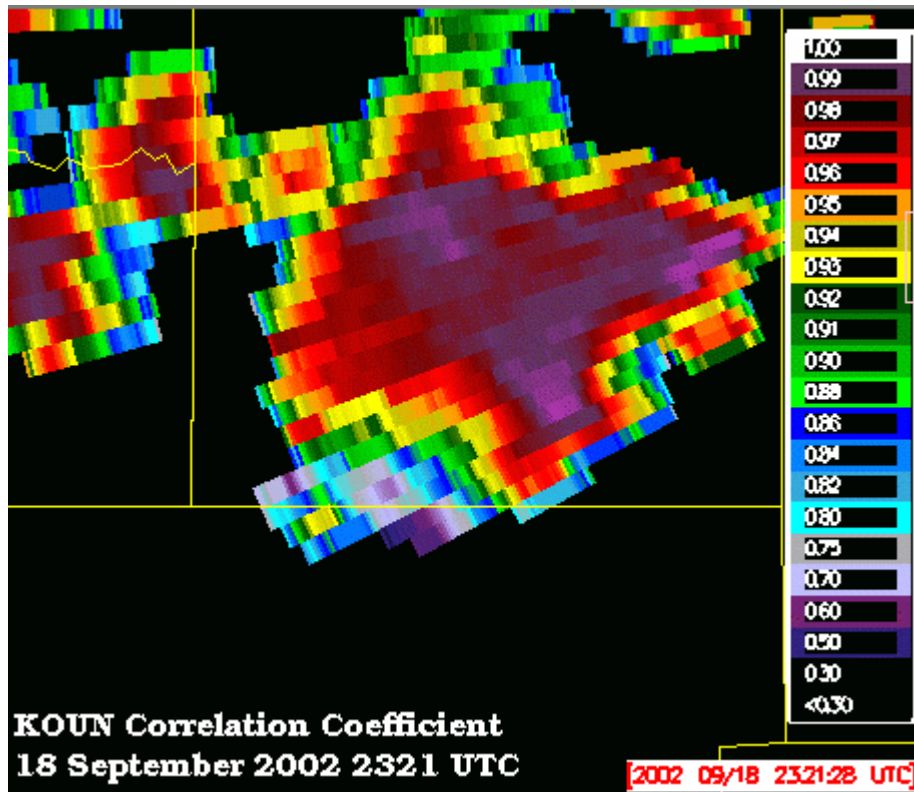


Figure 7. KOUN correlation coefficient at 18 September 2002 2321 UTC. View is toward the southwest. Very low values are coincident with the location of the reflectivity maximum in Fig. 3 and Z_{DR} “hole” in Fig. 4. This is another indicator of the presence of very large hail.

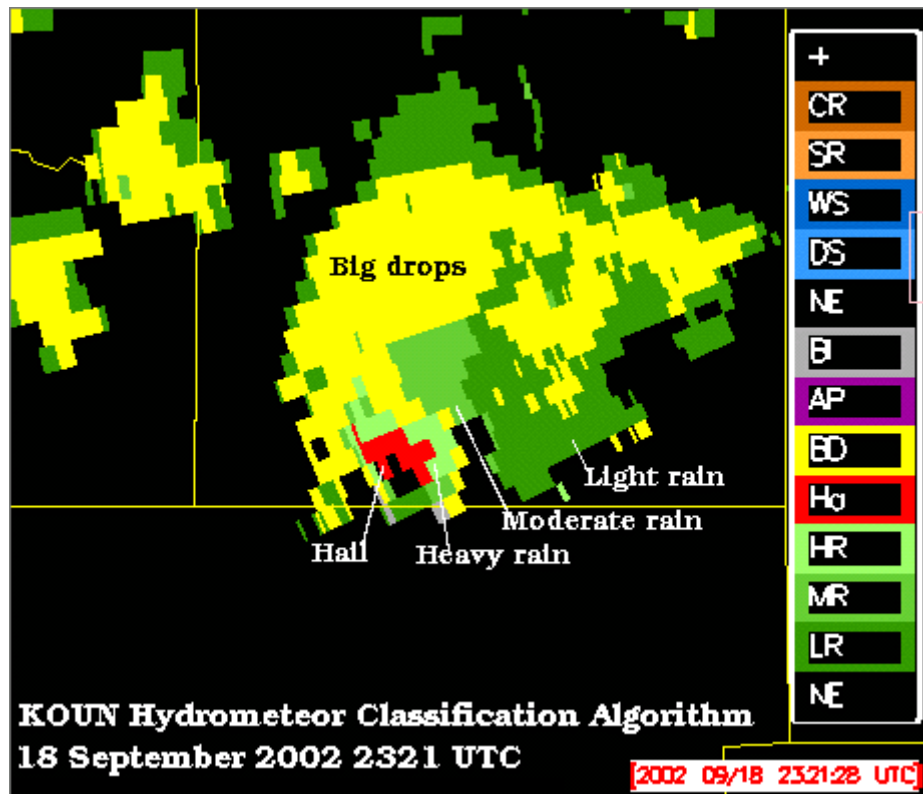


Figure 8. KOUN hydrometeor classification algorithm output at 18 September 2002 2321 UTC. The hail classification is consistent with the hail indicators in the base polarimetric products, and spotter reports of damaging 4.5-inch diameter hail.

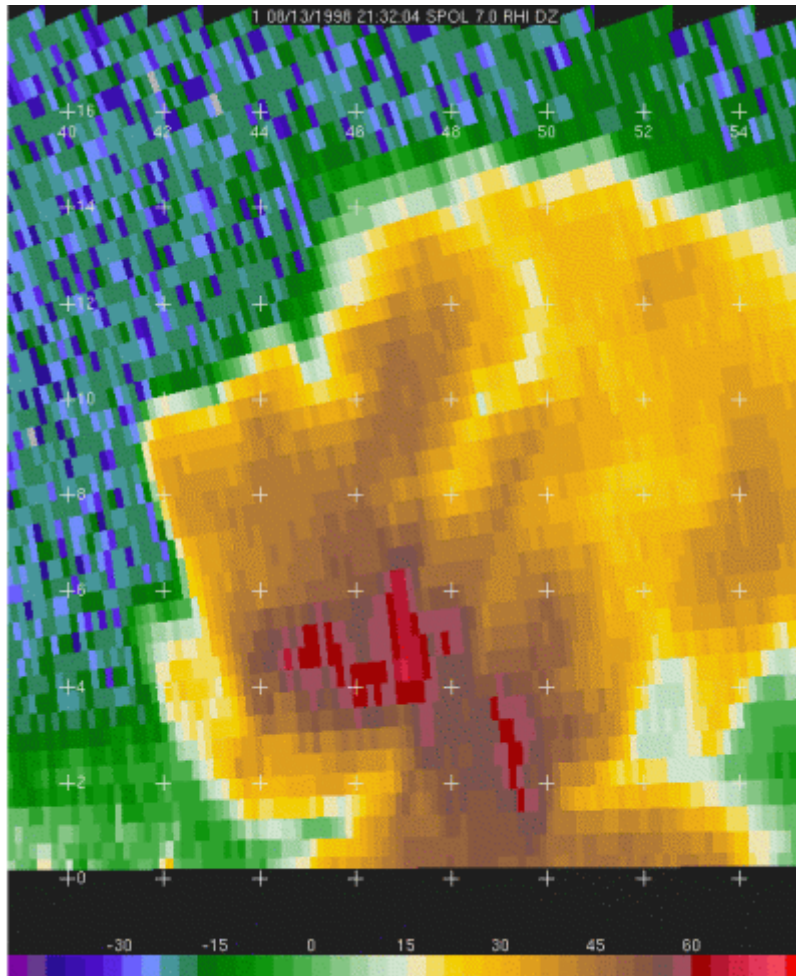


Figure 9. Cross-section reflectivity image of a severe thunderstorm as viewed by a research polarimetric radar. An elevated core of reflectivity in excess of 63 dBZ is evident 4-6 km above the ground.

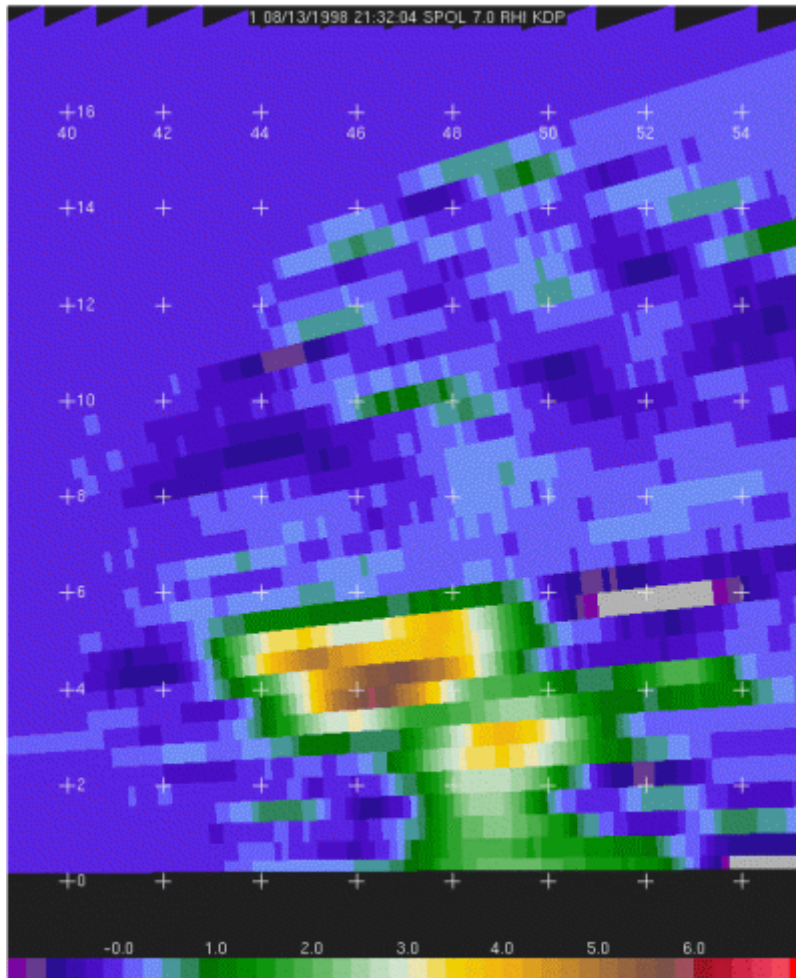


Figure 10. A cross section of specific differential phase (K_{DP}) corresponding to the reflectivity cross section in Fig. 9. Just below the level of highest reflectivity, a layer of very high K_{DP} is a clear indication of numerous water-coated hailstones. A damaging microburst impacted the ground below this layer. These polarimetric products suggest the downburst was driven by diabatic cooling from melting hail.

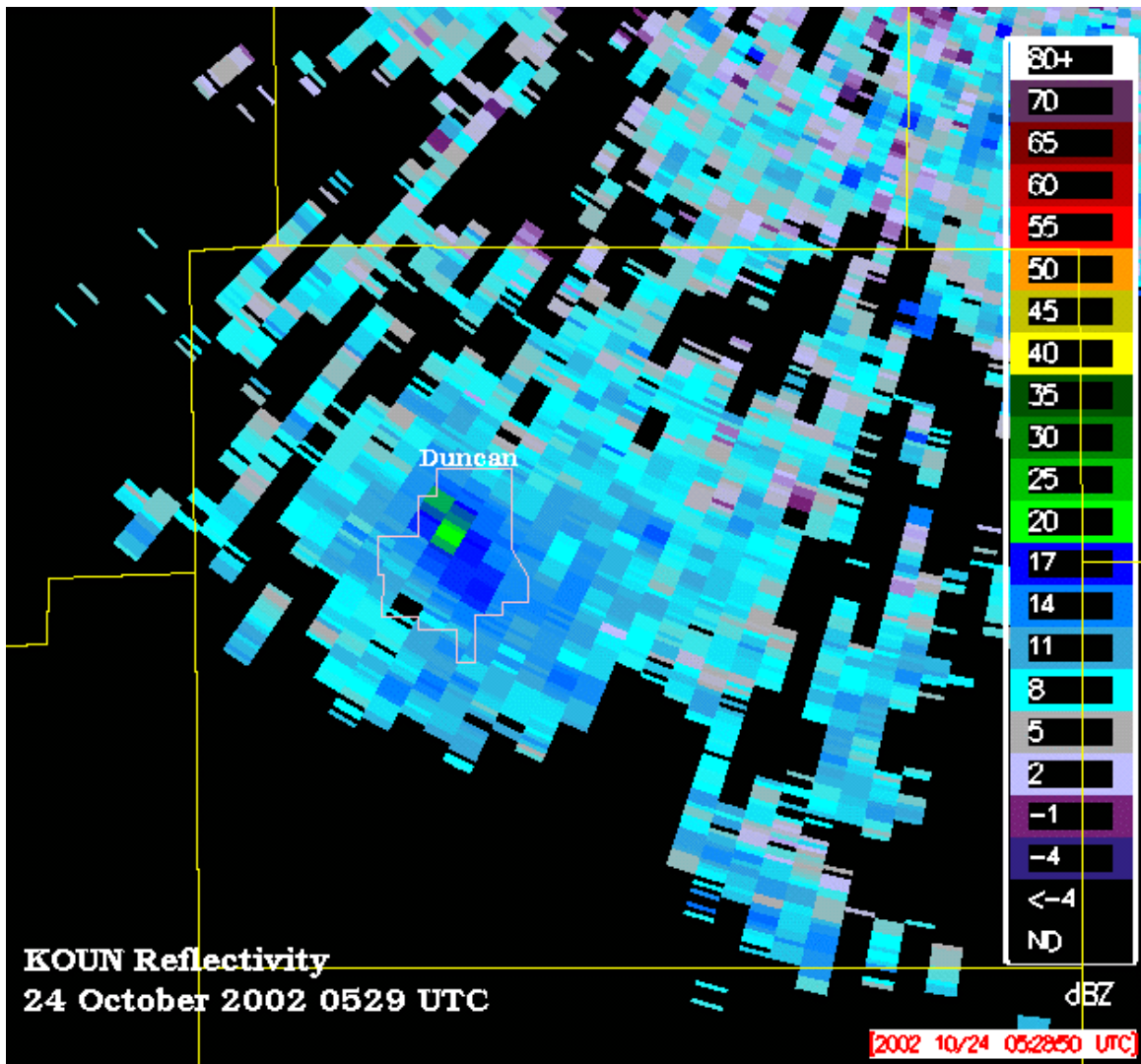


Figure 11. KOUN reflectivity at 24 October 2002 0529 UTC. A region of reflectivity above 20 dBZ moves directly over Duncan, Oklahoma.

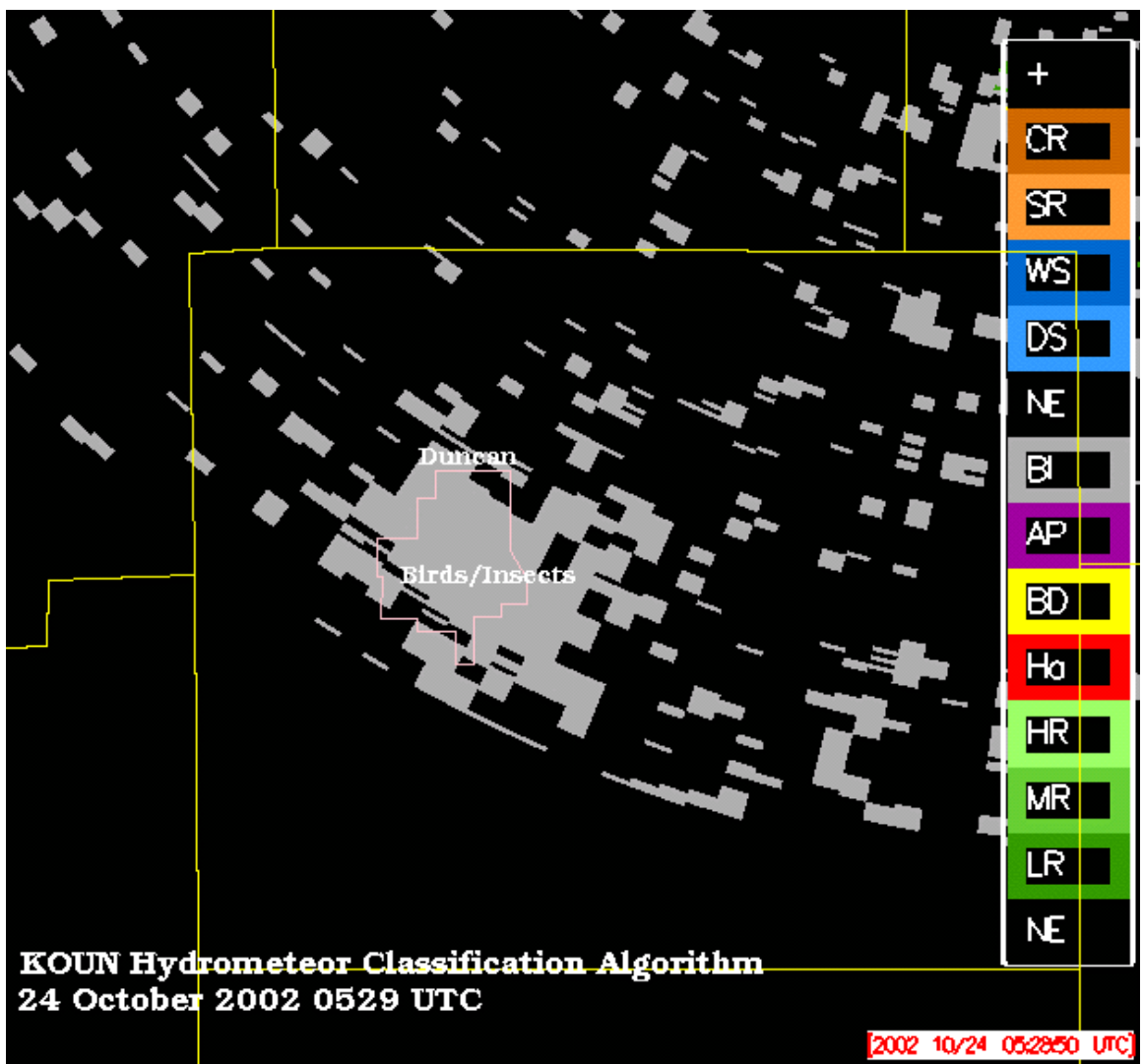


Figure 12. KOUN hydrometeor classification algorithm output at 24 October 2002 0529 UTC, corresponding to the reflectivity image in Fig. 11. While the presence of birds or insects over Duncan cannot be confirmed, two rain gauges in Duncan reported no precipitation during this period.

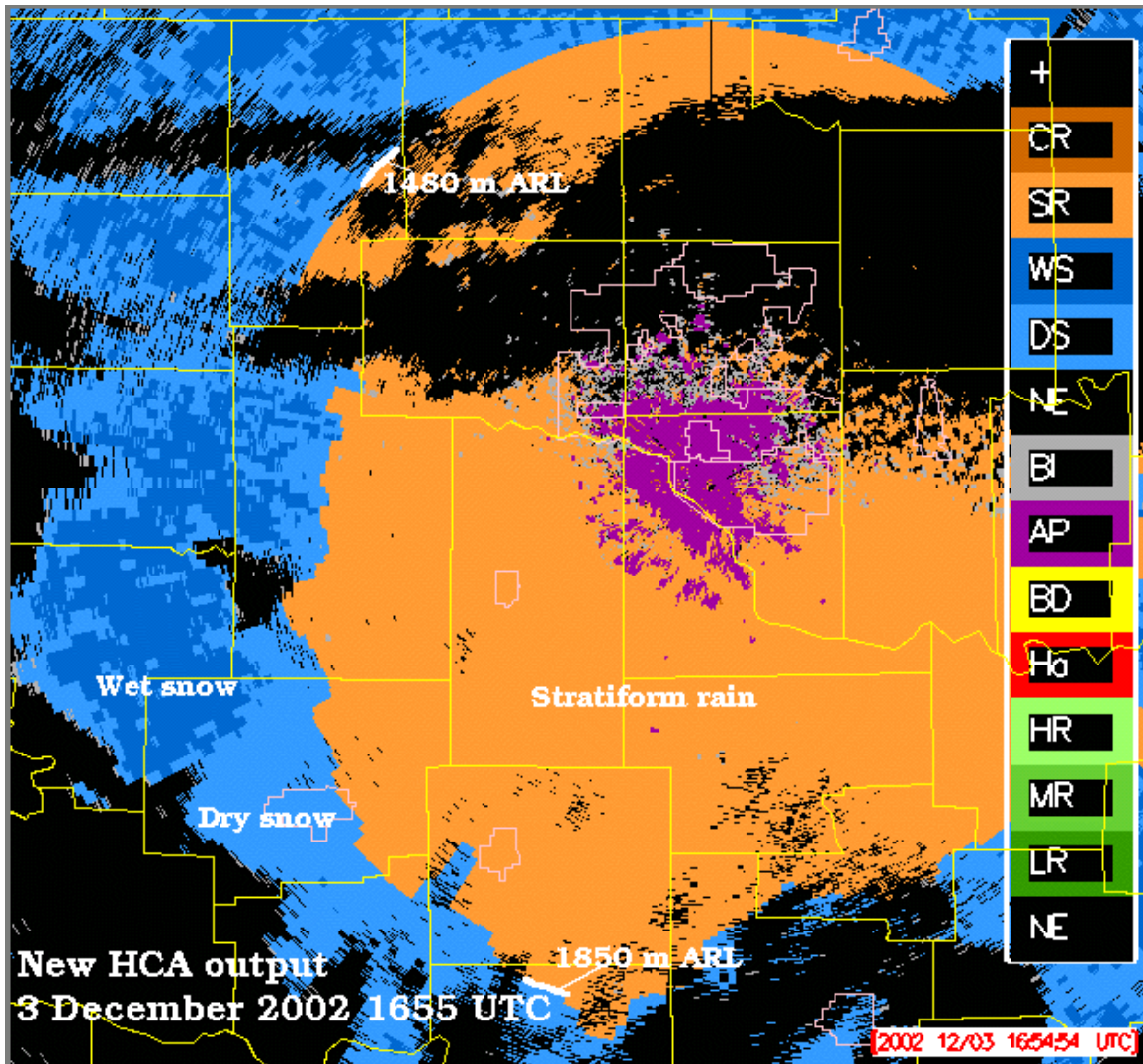


Figure 13. KOUN hydrometeor classification algorithm output at 3 December 2002 1655 UTC.

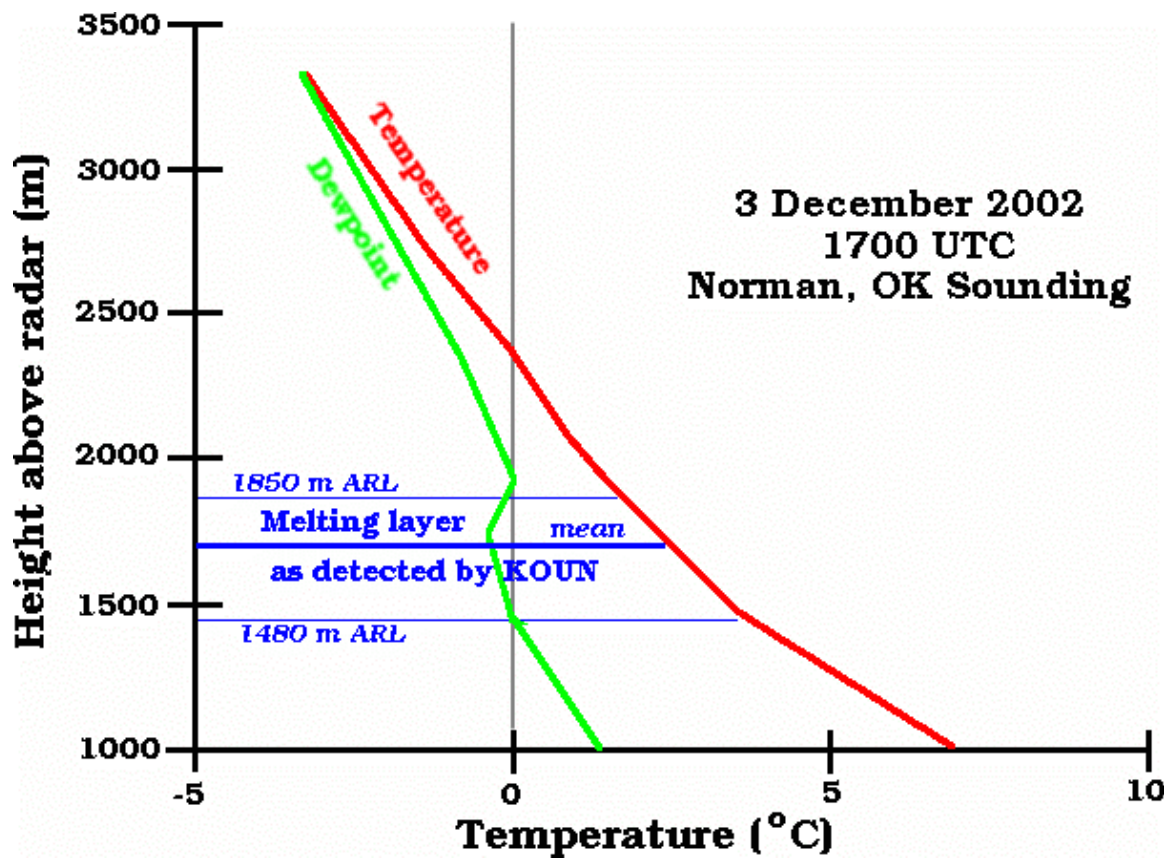


Figure 14. 3 December 2002 1700 UTC sounding from Norman, Oklahoma.

**IMPROVE II : Freezing Level Height
13 December 2001**

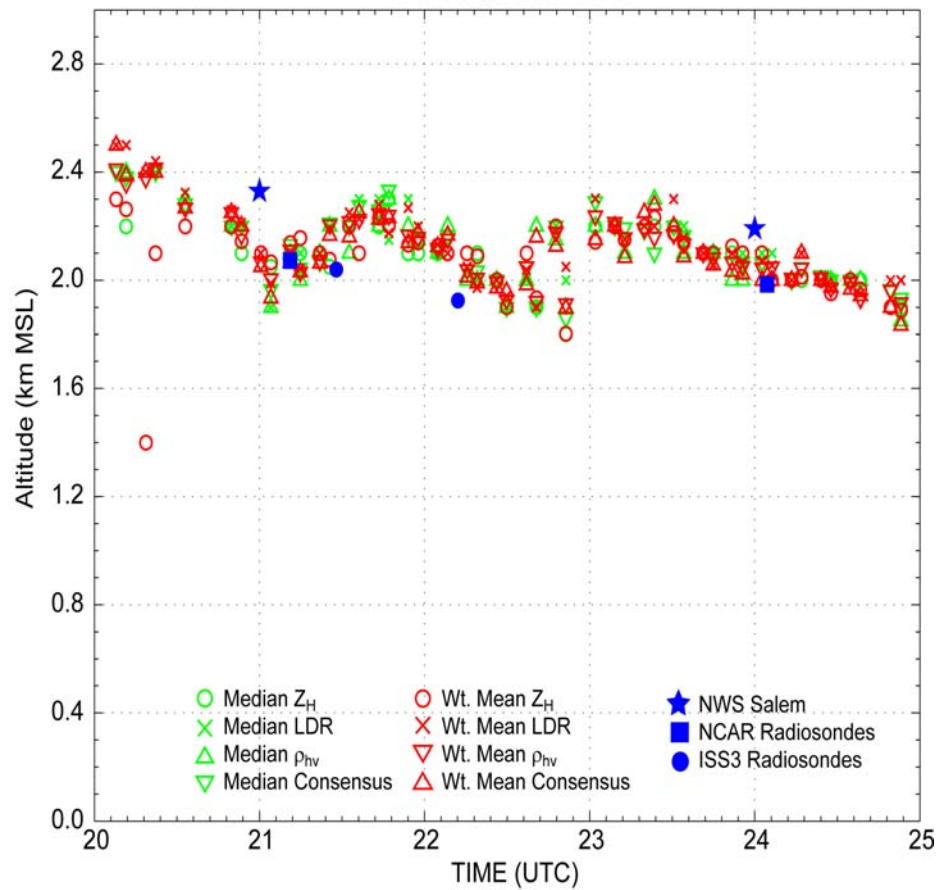


Figure 15. Freezing level retrievals based on radar reflectivity (Z_H), linear depolarization ratio (LDR), co-polar correlation coefficient (ρ_{HV}), and the consensus.

03.6.3 Circulations

Particularly violent or long-lived storms tend to possess certain notable qualities, including, for example, mesocyclones. The current WSR-88D algorithms have a very high false alarm rate. Controllers find such high false alarm rates unacceptable. To mitigate this problem, new more robust and reliable circulation detection algorithms will be developed. Algorithms that use circulations to diagnose storm severity or estimate storm longevity will be considerably improved by this work.

a) Current Efforts

NSSL has implemented a local, linear, least-squares method for calculating derivatives of Doppler radial velocity data. This method uses a range-dependent kernel size to estimate the divergent and rotational components of the radial velocity field. This Linear Least Squares Derivative (LLSD) technique is more robust and stable than earlier methods of calculating azimuthal shear and radial convergence, such as those implemented in NSSL's single-radar Mesocyclone Detection Algorithm. The LLSD method allows velocity derivatives from multiple radars to be easily merged and for these important data fields to be viewed in 3-dimensional space, which is not possible with radial velocity data.

During Q1, NSSL tested the LLSD technique in real-time during severe weather episodes in the southeast US (Fig. 16). NSSL is also testing three-dimensional, multi-radar merged fields of LLSD rotational shear and divergence in real-time.

b) Planned Efforts

Investigate characteristics of the radial derivative field (pseudo convergence) and determine methods for extracting relevant information about storms for the combined rotational and convergent shears. The k-means clustering method will be investigated for this purpose. In addition, merge LLSD output into a 3D gridded product from multiple radars.

c) Problems/Issues

None.

d) Interface with other Organizations

None.

e) Activity Schedule Changes

None.

03.6.4 Technical Facilitation

Technical facilitation supports the NEPDT algorithm development. There is currently no standard vehicle outside of NSSL for algorithm development support. The interface being developed at the NSSL, the WDSS-II, provides a way to develop, validate, verify and demonstrate the NEXRAD algorithms developed within this PDT. Additionally, WDSS-II provides a route into the Open Radar Product Generation (ORPG) system. WDSS-II will support and incorporate the MITRE Common Operations Development Environment (CODE). WDSS-II is an important ingredient for the overall success of the NEPDT because, in consonance with CODE, coding and testing standards at the application prototype level are enforced. Transfer of single-radar algorithms to the ROC will be straightforward, as anything within WDSS-II must also conform to CODE standards. Overall, NEPDT efforts will inevitably enhance the algorithms that have been accepted or will be implemented by the ROC as part of the WSR 88D system.

a) Current Efforts

(1) Developed tools for merging data from multiple sensors and algorithms using different strategies such as distance-blending, time-and-distance blending, and internally advecting the data from different sensors to the time of the combined grid (Figs. 17, 18, 19 and 20).

This makes use of statistical clustering to find storms, a Kalman estimator to keep a running estimate of velocity and acceleration/deceleration and corrections applied to the fields to advect them. The same technique can be used to make field forecasts over short periods of time. For example, this is a 30-minute forecast (Fig. 21):

(2) Developed capability to use terrain data to infer beam blockage. The terrain blockage information is also used in the merger of data, by using data from radars that are not blocked (and which, therefore, may be further away).

(3) Implemented interactive storm-motion correction of velocity measurements (Fig. 22).

(4) Solved problems related to extra, straggling radials when radar hiccups. These cropped up in real-time tests at Jackson, MS.

(5) Cross-sections now update whenever a single new tilt comes in.

(6) Support was added for additional, experimental VCPs.

b) Planned Efforts

Continue work on supporting model and satellite data for input to algorithms.

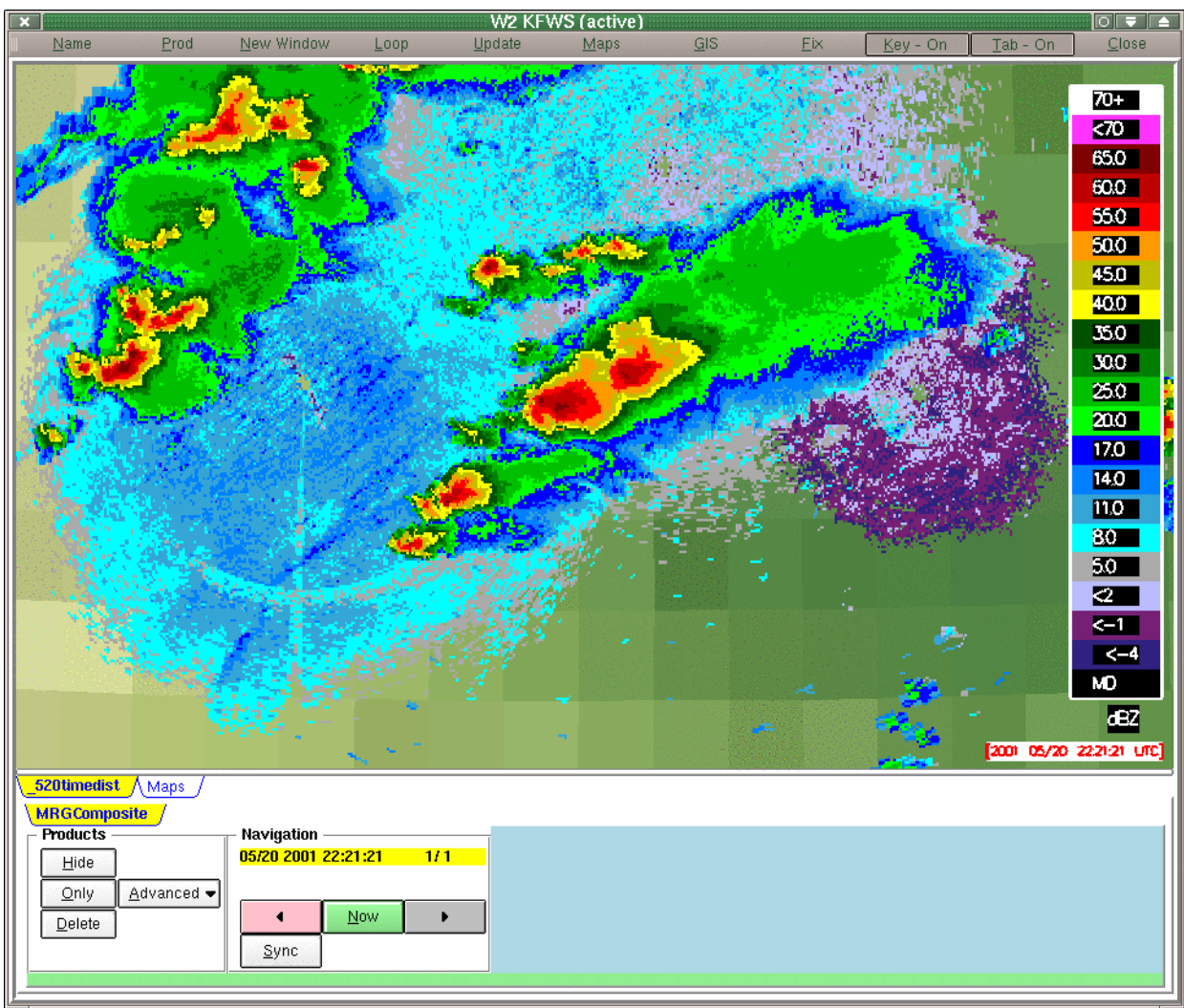


Figure 17. Radar data merging based on time-and-distance weighting.

c) Problems/Issues

None.

d) Interface with other Organizations

None.

e) Activity Schedule Changes

None.

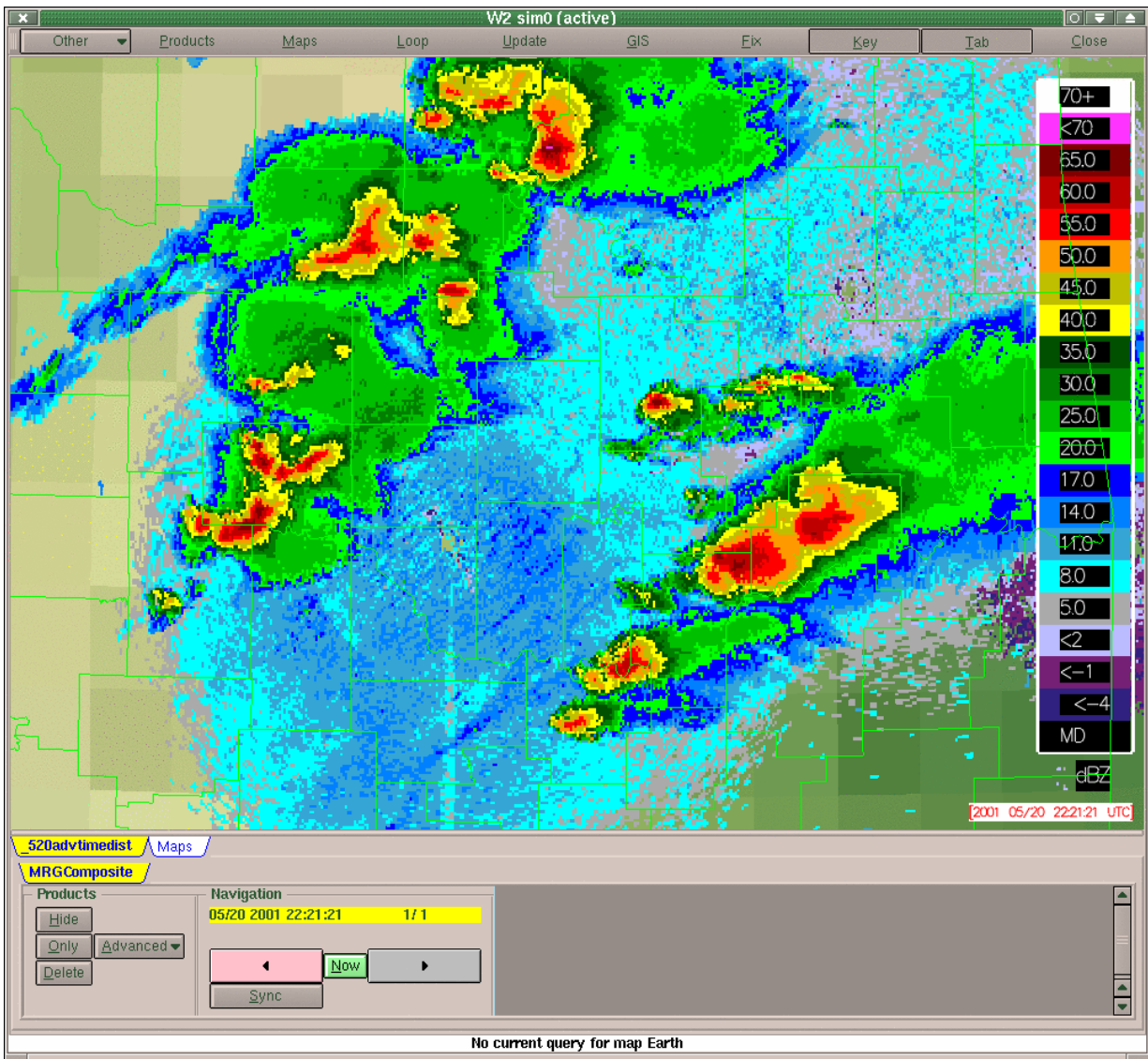


Figure 18. Merging after time-matching the data.

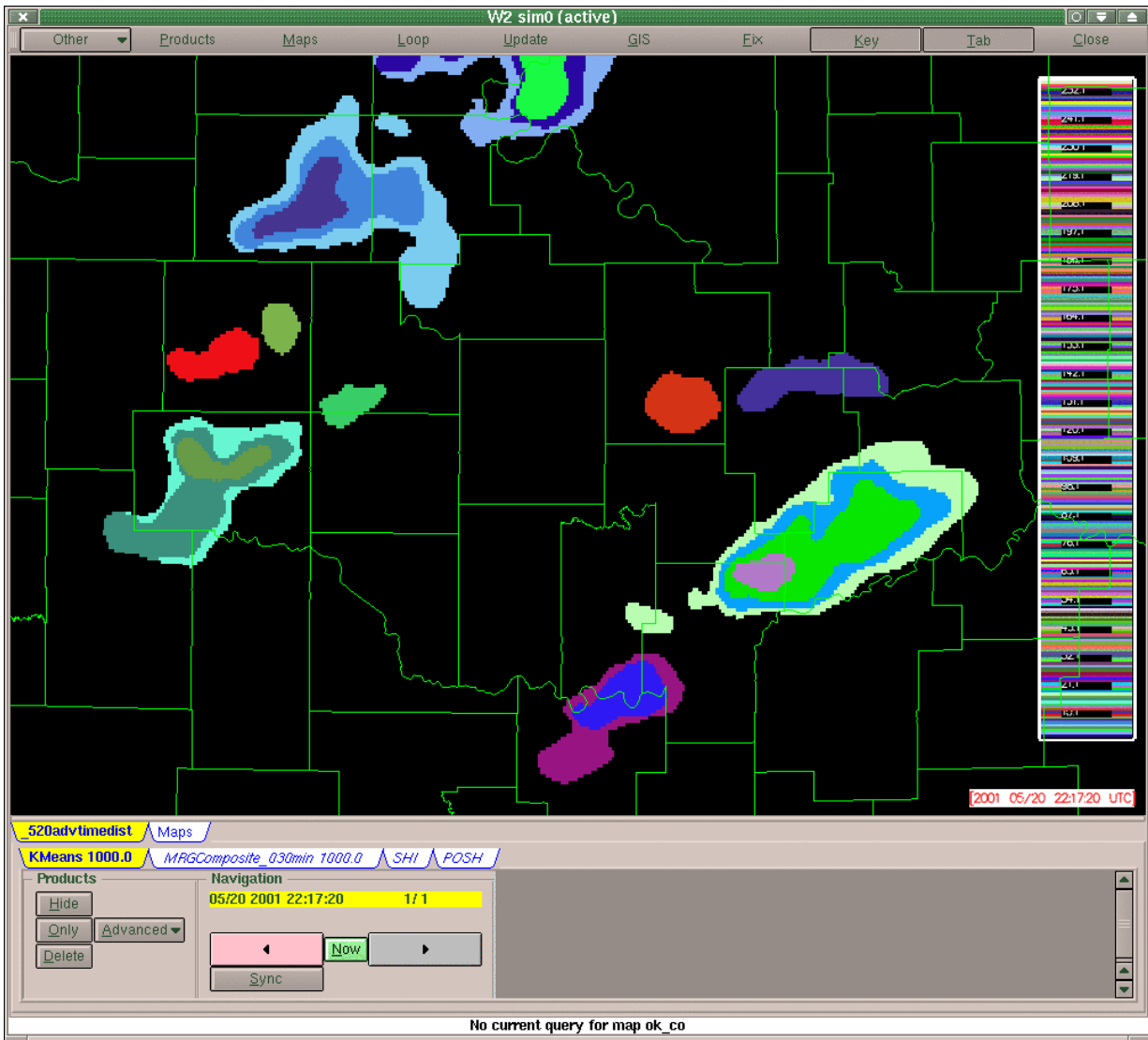


Figure 19. Storms identified via k-means clustering in the merged grid.

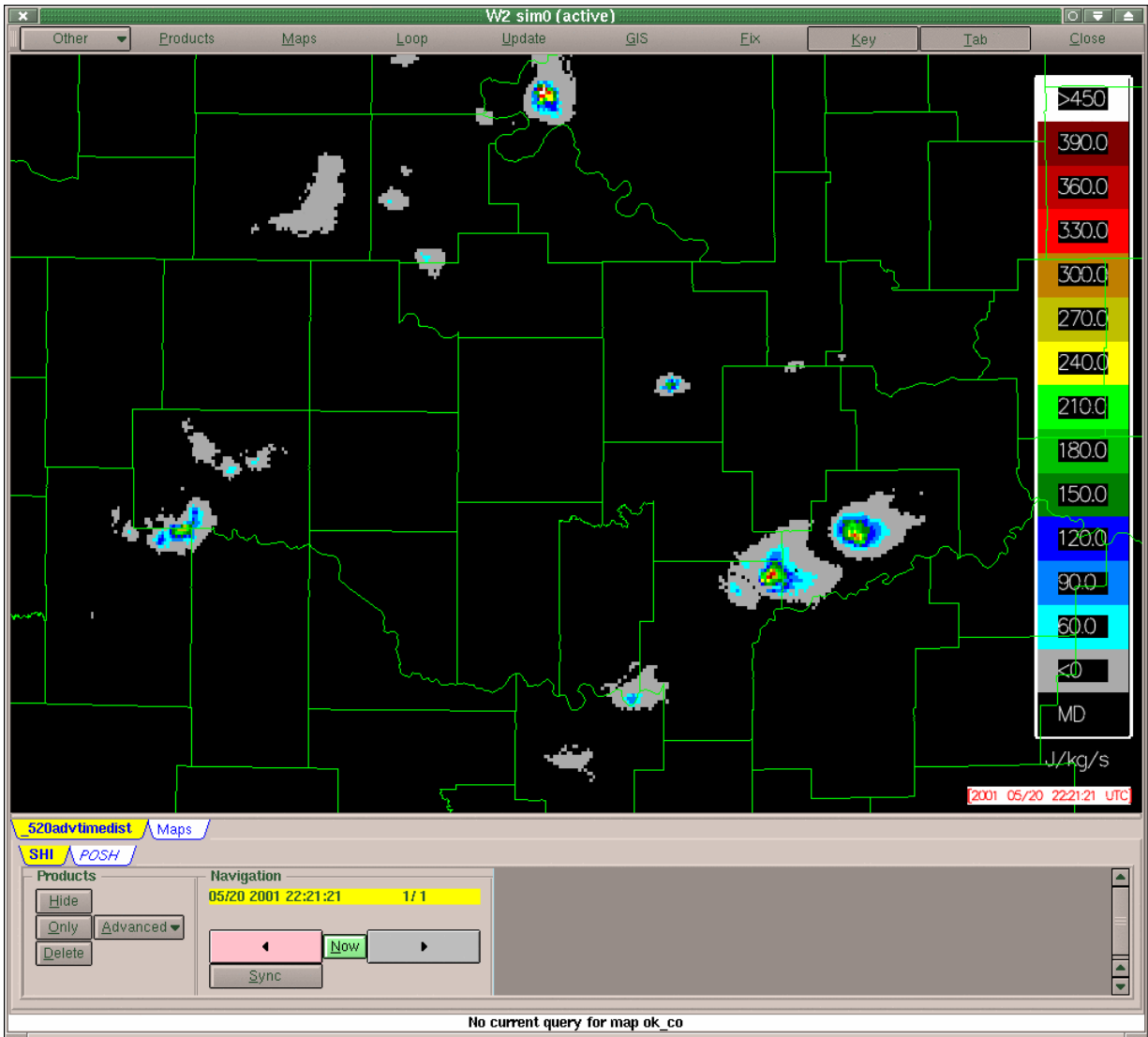


Figure 20. Severe Hail Index computed on the merged grid.

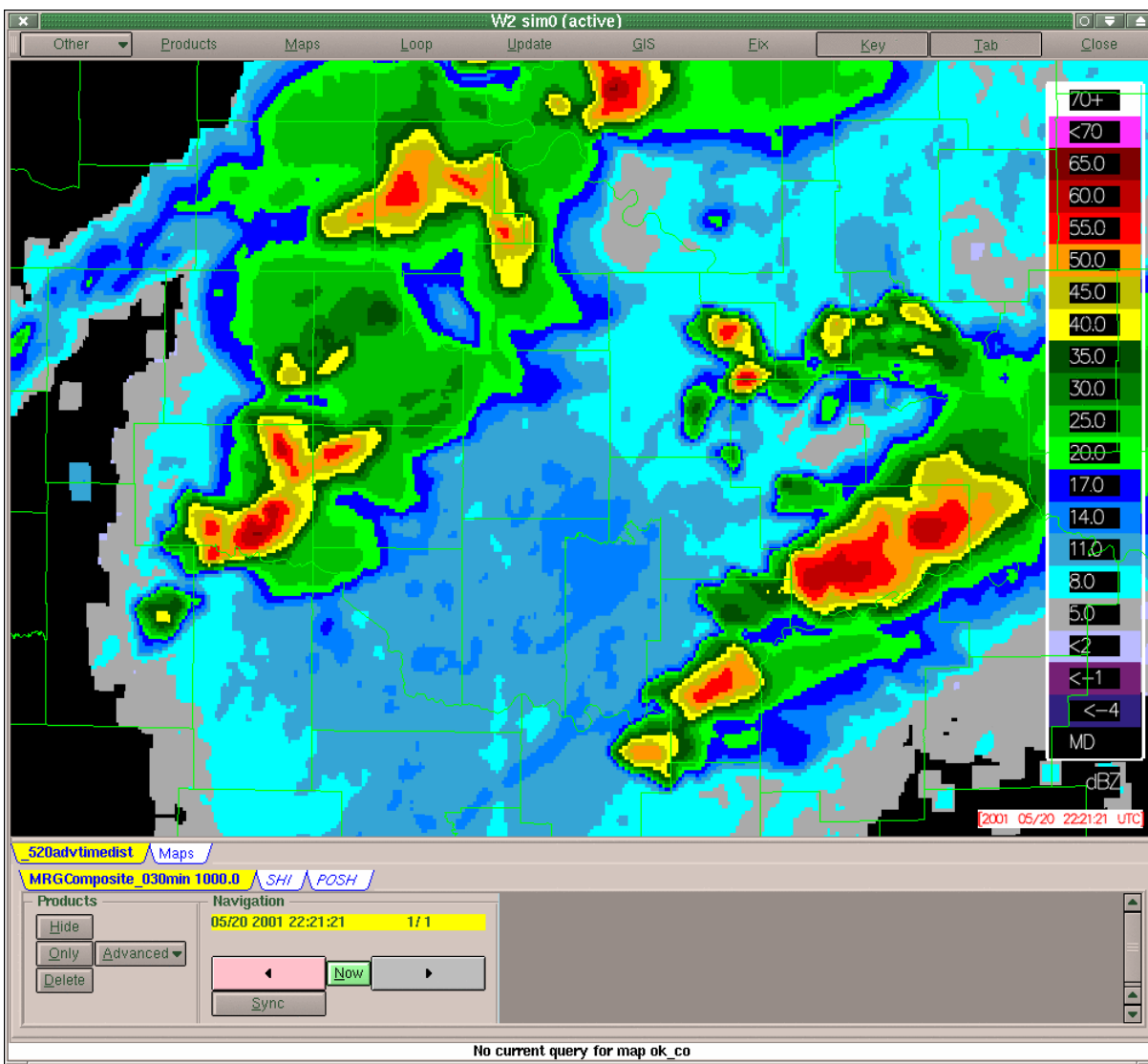


Figure 21. Example of forecast storm positions and intensities based on Kalman-filtered, non-linear advection and trending applied to storms identified with k-means clustering.

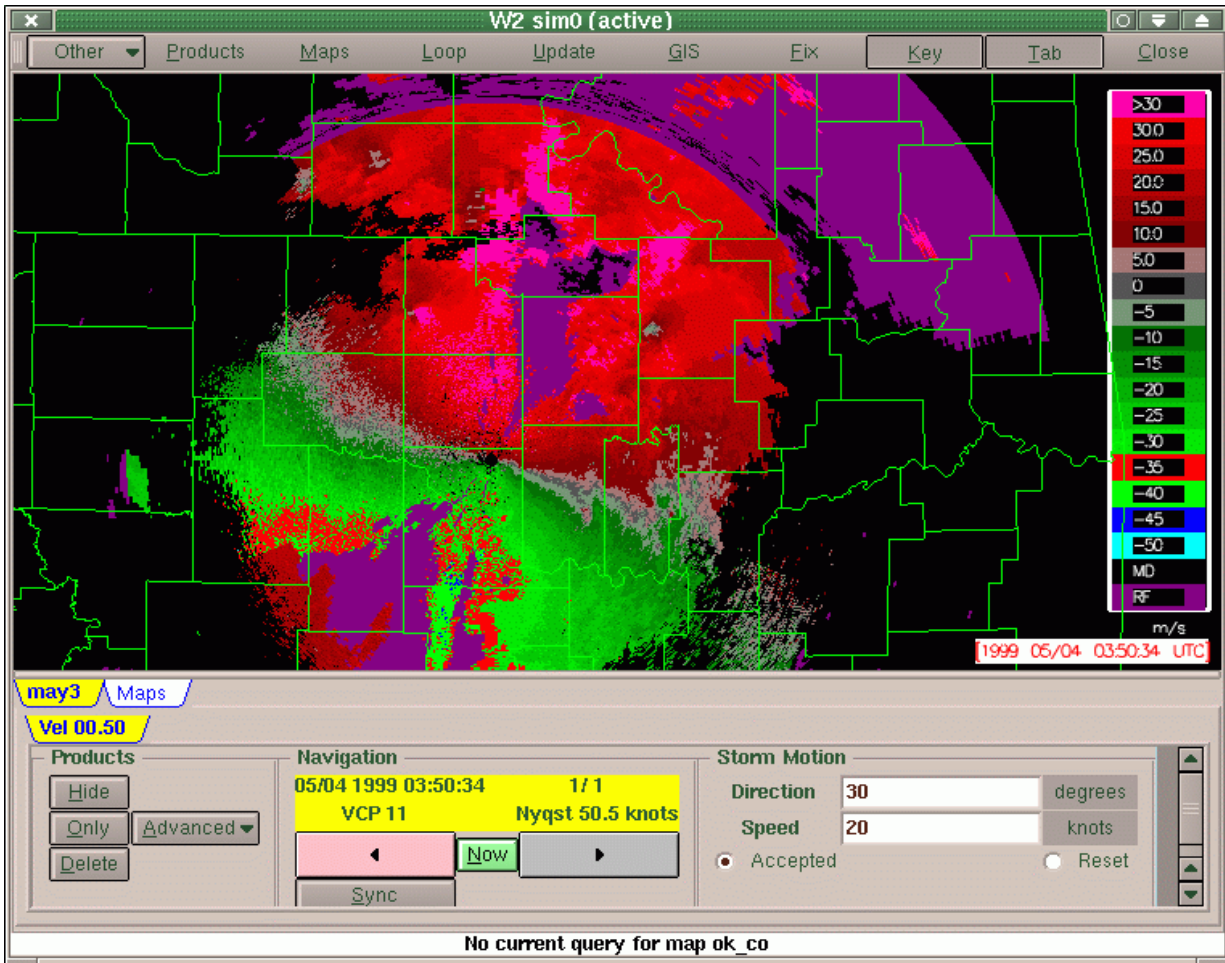


Figure 22. Storm motion adjustments applied to velocity field to yield storm-relative velocity. The applied correction varies as a function of position and is not constant.

03.6.12 Product Implementation

Product implementation is a the process by which implementation paths are explored and defined within the aviation community systems that are best for NEPDT products. This process includes collaboration with other PDTs to help define the nature of WSR-88D they need. Technical facilitation also includes the low-level process of defining technical details (formats, data set file structures, etc.) of the products developed NEPDT.

a) Current Efforts

Work with NCAR on collecting, archiving, and disseminating 3D reflectivity grids for an East Coast winter storm that occurred in early December. In addition, the Level II velocity data for this case has also been made available. The 3D gridded radar data is now available routinely via ftp download. A rolling archive of the previous 5 days has also been made available.

The process of reanalyzing several days of convective weather within the CIWS region has begun. These data will be made available to any and all AWRP PDTs via ftp.

b) Planned Efforts

As a result of meetings held in Boulder in early December, an NEPDT program review is being planned. The program review will focus on the 3D gridded reflectivity product. A complete, detailed discussion of the technique chosen for this product will ensue, along with examples of alternative techniques. The program review is tentatively planned for a single day in early April, and may include other topics if interest is sufficient.

c) Problems/Issues

None.

d) Interface with other Organizations

NCAR, MIT/LL, FSL.

e) Activity Schedule Changes

None

03.6.14 Multi-radar Composites

The area for which any arbitrary ARTCC has responsibility likely encompasses the coverage area of several WSR-88D installations. Neither the ROC nor the NWS has plans to treat the various WSR-88D installations as a single network, so there are no existing algorithms that use data from more than one radar. This is a serious limitation, because treating each radar separately leads to ambiguities when the radar data overlap. Currently, the users must independently mitigate these ambiguities, which requires significant knowledge about meteorological radar data and the nature of the algorithms that are run on these data. Aviation users generally do not possess this knowledge, so for the WSR-88Ds to be treated as a network, algorithms and techniques aimed specifically at multiple radar composites must be developed.

a) Current Efforts

03.6.14.1 Continued test of real-time 3-D mosaic for the FAA CIWS region

The activities for this quarter include continued monitoring and testing of the real-time 3-D mosaic for the CIWS domain and work with the CWPDT and the WWRPDT on the use of the CIWS mosaic grid data.

The real-time 3D mosaic has been running stably since the installation (Aug. 30, 2002). The mosaic grid data are kept online for two-days at a public ftp site. An anonymous ftp account (with IP address restrictions) has been set up for users (e.g., CWPDT or WWRPDT) to retrieve real-time data. A couple of winter storm cases are archived for further study (by WWRPDT).

The CWPDT has identified a few convective storm cases that occurred before Aug. 30, 2002 and the 3D mosaic will be re-run for those cases. During this quarter we are continuing to collect the level-II data from all CIWS domain radars for the identified cases.

03.6.14.2 Improvement and refinement of the real-time 3-D mosaic for the CIWS region(s).

(This task starts at Jan.1, 2003.)

03.6.14.3 Prototype the strategies for displaying the SSAP products together with the 3-D reflectivity mosaic.

(This task starts at Mar.1, 2003.)

03.6.14.4 Collect SSAP products for prototype display and refine the product data format based on requirement of display systems.

(This task starts at July 1, 2003.)

03.6.14.5 Develop least-square fitting algorithm (Elmore et al. 1993) for deriving radial and azimuthal wind-shear fields from single radar velocity fields.

The initial code for the least-square fitting algorithm has been developed and is under testing.

03.6.14.5 Generate single radar wind-shear fields for selected cases.

(This task starts at Jan. 1, 2003.)

03.6.14.6 Remap single radar wind-shear fields onto the 3D mosaic grid.

(This task starts at Apr. 1, 2003.)

03.6.14.8 Investigate various data structures and physical algorithms for a four-dimensional dynamic data analysis and visualization system. The system will continuously ingest data from different sources (e.g., radar, satellite, lightning, and others) and produce continuously updating 3-D, high-resolution data grids on a regional-scale.

A general radar data gridding and mosaicking system has been under investigation. The current 3D multi-radar mosaic runs at discrete time levels on clock and it populates a 3D Cartesian grid with the latest volume scans from different radars. There is no temporal weighting scheme in the mosaic, so all the latest volume scans are assumed to be valid at the time of the mosaic. This system is not optimal for TDWR data since the TDWR scans have repetitive tilts in a volume scan. Table 1 shows the OKC TDWR's hazardous scan strategy. In one

Table 1. TDWR Hazardous Scan Strategy

Tilt #	1	2	3	4	5	6	7	8	9	10	11	12
Elevation Angle (°)	0.6	0.3	0.3	3.8	7.5	11.2	0.3	1.0	14.6	19.2	0.3	24.9
Tilt #	13	14	15	16	17	18	19	20	21	22	23	
Elevation Angle (°)	31.8	3.8	0.3	7.5	11.2	14.6	0.3	19.2	24.9	31.8	0.3	

volume scan, the radar scans at 0.3° for 7 times and scans at each of the 3.8, 7.5, 11.2, 14.6, 19.2, 24.9, and 31.8° elevations twice. With the current mosaic, only the last 0.3° tilt data would be used in the final grid and so do the other repetitive tilts. For users who need very rapid update at the lower levels (e.g., near the airport), important observations could be lost. To alleviate this problem, the 3D mosaic system can be modified and a new tilt-based, continuous update mechanism can be developed.

The new system will start with an empty 3D Cartesian grid. When the first tilt from any of the radars that cover the grid become available, the data will be mapped onto the proper grid cells in the domain and the time is recorded. When the next tilt of data come in (which could be from a different radar than the first one), the new data will be mapped on to the associated grid cells. At the grid cells where old data exist, the new and old data will be combined using a weighting function that depends on the space (range to radar) and the time. Since the gridding and mosaicking processes are now running dynamically (based on the arrival of new data, not on clock) and have temporal weighting component, we'll call the new system a "four-dimensional dynamic grid" (FDDG).

The spatial weighting functions in the 3D mosaic system can be used for the FDDG system since they have been well tested using many cases. The temporal weighting function will need to be developed and tested using case studies. One of the advantages of the FDDG is that the different users can extract the 3D reflectivity mosaic grid at different time scales as they would need. For instance, the current 3D mosaic users can still get the regional reflectivity grid every 5 or 10 minutes. And the new mosaic grid will be more representative of the time evolution of the weather systems than the current mosaic grid if proper temporal weighting functions are used. With the time dimension, the FDDG system will also open the opportunity for motion adjustments to the reflectivity mosaic filed.

03.6.14.9 Develop feasible strategies for the 4-D dynamic data updating system.

(This task starts at Apr.1, 2003.)

03.6.14.10 Begin development of an initial and prototype 4-D dynamic data updating system based on the proposed strategies.

(This task starts at July 1, 2003.)

b) Planned Efforts

For the next quarter, the case study with the CWPDT will be continued. Based on the requirements from the WWRPDT, the ftp access will be enhanced (adding the radial velocity data and increase the time length of the online data). Continued development of the least-square fitting algorithm for wind-shear fields. The 3D mosaic will be further improved and the development of a prototype 4-D dynamic grid will begin.

c) Problems/Issues

None.

d) Interface with other Organizations

Worked with Winter Weather Research PDT on the ftp access of the 3D mosaic data for the CIWS domain.

e) Activity Schedule Changes

None.

03.6.15 WARP Activities

The WARP is integral to AT controller displays. Warp is significant in that it shifts the burden of displaying weather radar returns to an instrument specifically designed as a weather radar: the WSR-88D. However, due to the nature of its mission and hardware, the WSR-88D cannot take the same approaches to data quality control as do the long-range L-band radars currently used by ATC. New approaches to data quality control need to be developed so the users have confidence in the weather data products displayed to them.

a) Current Efforts

The focus of NSSL's work in support of WARP has recently changed to provide the National Air Traffic Controllers Association (NATCA) with guidance on the accuracy of ORPG composite reflectivity products. The FAA has decided to use ORPG product 96 (0-70,000 ft composite reflectivity with AP mitigation) to replace product 36 (0-70,000 composite reflectivity without AP mitigation) on the WARP Display System Replacement (DSR) in the Spring of 2003. NSSL will provide guidance on the accuracy of the AP mitigation scheme in product 96 for a variety of meteorological environments. ORPG software has been successfully modified to produce quantitative performance measures that assess the accuracy of the AP mitigation scheme. The performance metrics are identical to those originally used by Lincoln Labs including the probability of editing AP (PEAP) and probability of editing weather (PEW). PEAP is the number of AP pixels correctly edited divided by the total number of AP pixels. PEW is the number of weather pixels edited divided by the total number of weather pixels. The goal is to obtain a high PEAP and a low PEW. PEAP and PEW are only calculated for reflectivity pixels with a value greater than or equal to 30 dBZ since the WARP DSR only displays reflectivities above 30 dBZ.

Figs. 23 and 24 show a strong nocturnal AP event near Amarillo, Texas that occurred on April 18, 2002. Severe AP returns exist southwest of the KAMA radar site. The AP mitigation scheme is not able to remove much of the AP beyond 148 km because of the lack of velocity and spectrum width data. There are 4256 pixels or data bins of reflectivity greater than or equal to 30 dBZ. Only 26 of these are weather pixels and 100% of them are identified as precipitation returns giving a PEW of 0%. Thus 4230 pixels are clutter returns with 2475 of those incorrectly diagnosed to be weather. So the PEAP is only 41.5%.

If only reflectivity pixels with corresponding velocity and spectrum width data are considered, the PEAP increases to 83.5%. Thus, the problem of not having all 3 moments of radar data is the main problem for the poor performance of the AP mitigation scheme in this case.

In addition to examining AP events, NSSL will also look at convective events with no AP to determine how over-aggressive the AP scheme may be at reducing the magnitude of reflectivity returns associated with convective cells. An

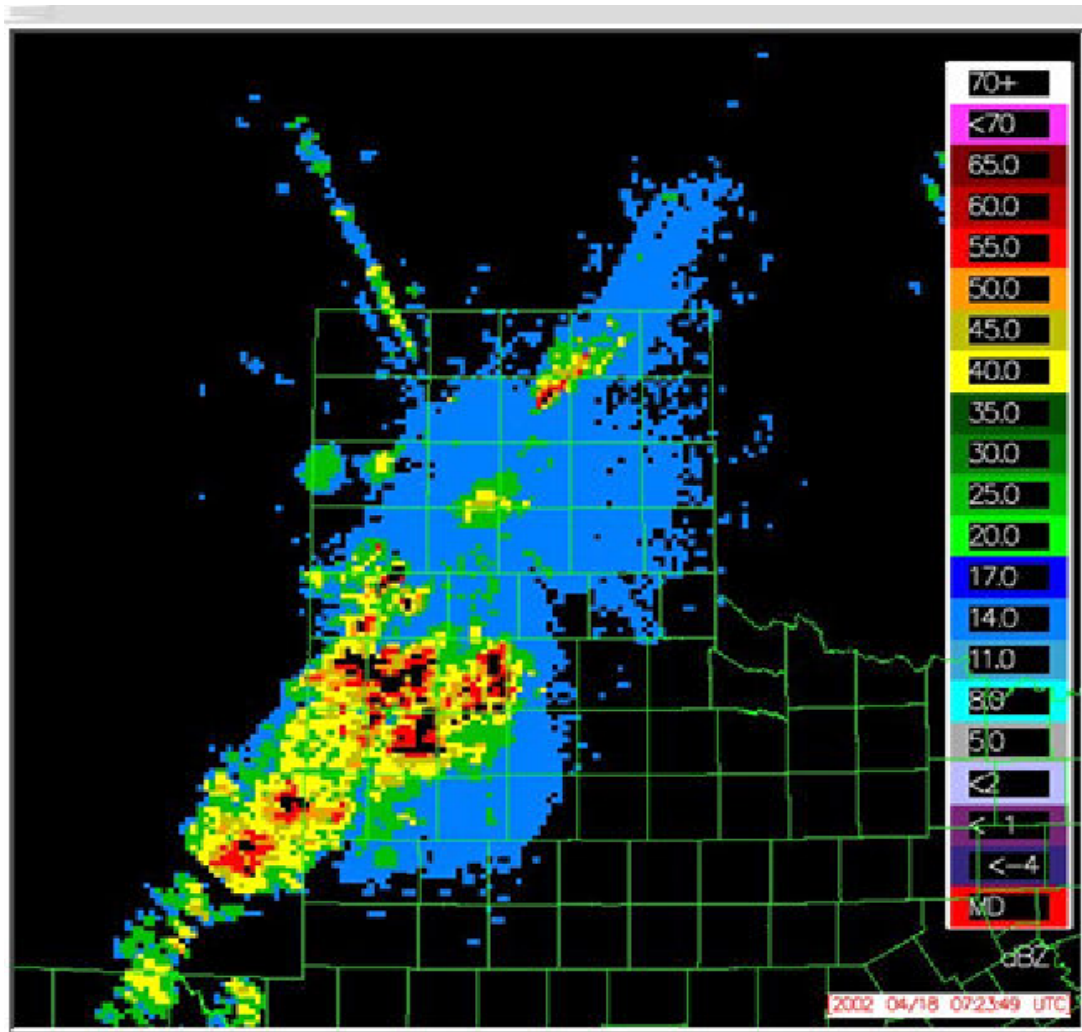


Figure 23. Composite Reflectivity (8 data levels, 2 n mi resolution – ORPG Product 36) at KAMA April 18, 2002, 0724 UTC. This is a nocturnal AP event with extensive, very strong returns of over 50+ dBZ southwest of Amarillo.

example is shown in Figs. 25 and 26. When the AP scheme is applied in this case, reflectivity values associated with several convective cells are reduced to near 30 dBZ. Thus, those convective cells would disappear from the WARP DSR display since no reflectivity returns below 30 dBZ are displayed to air traffic controllers. The AP scheme is over-aggressive in this instance with unfortunate implications for air traffic controllers and pilots. A subjective and quantitative evaluation of ORPG composite reflectivity products with and without AP removed that are used by WARP will continue. Cases are being analyzed and archived at <http://www.nssl.noaa.gov/~porter/warp/cr>.

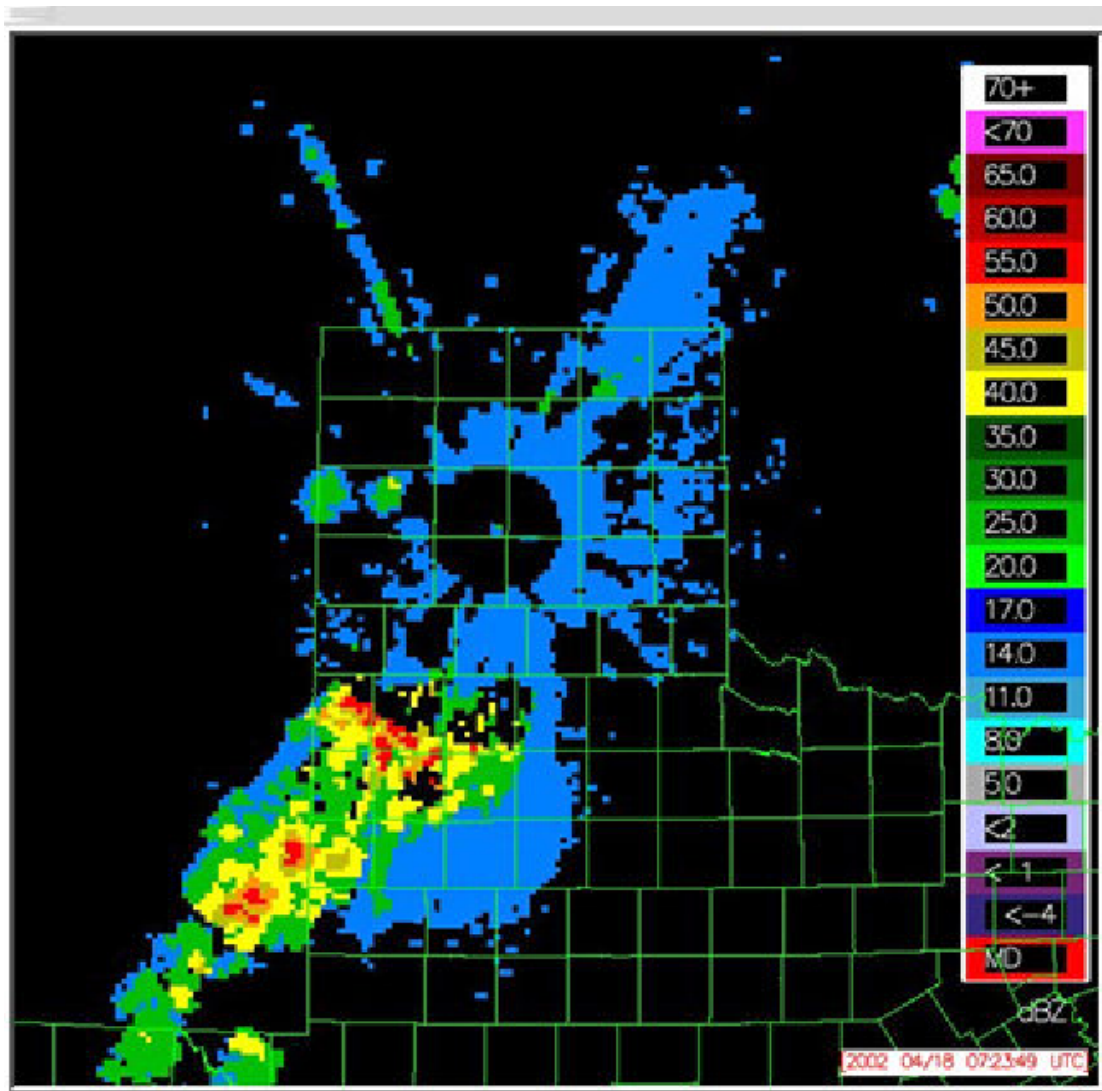


Figure 24. Composite Reflectivity with AP Edited (8 data levels, 2 n mi resolution – ORPG Product 96) at KAMA April 18, 2002, 0724 UTC. Clutter immediately surrounding the radar is removed, however, most of the AP to the southwest remains because all 3 moments of radar data are not available at that range.

b) Planned Efforts

Continue analysis of Product 96 performance statistics for cases that have already been collected and are on-hand at NSSL.

c) Problems/Issues

None.

d) Interface with other Organizations

None.

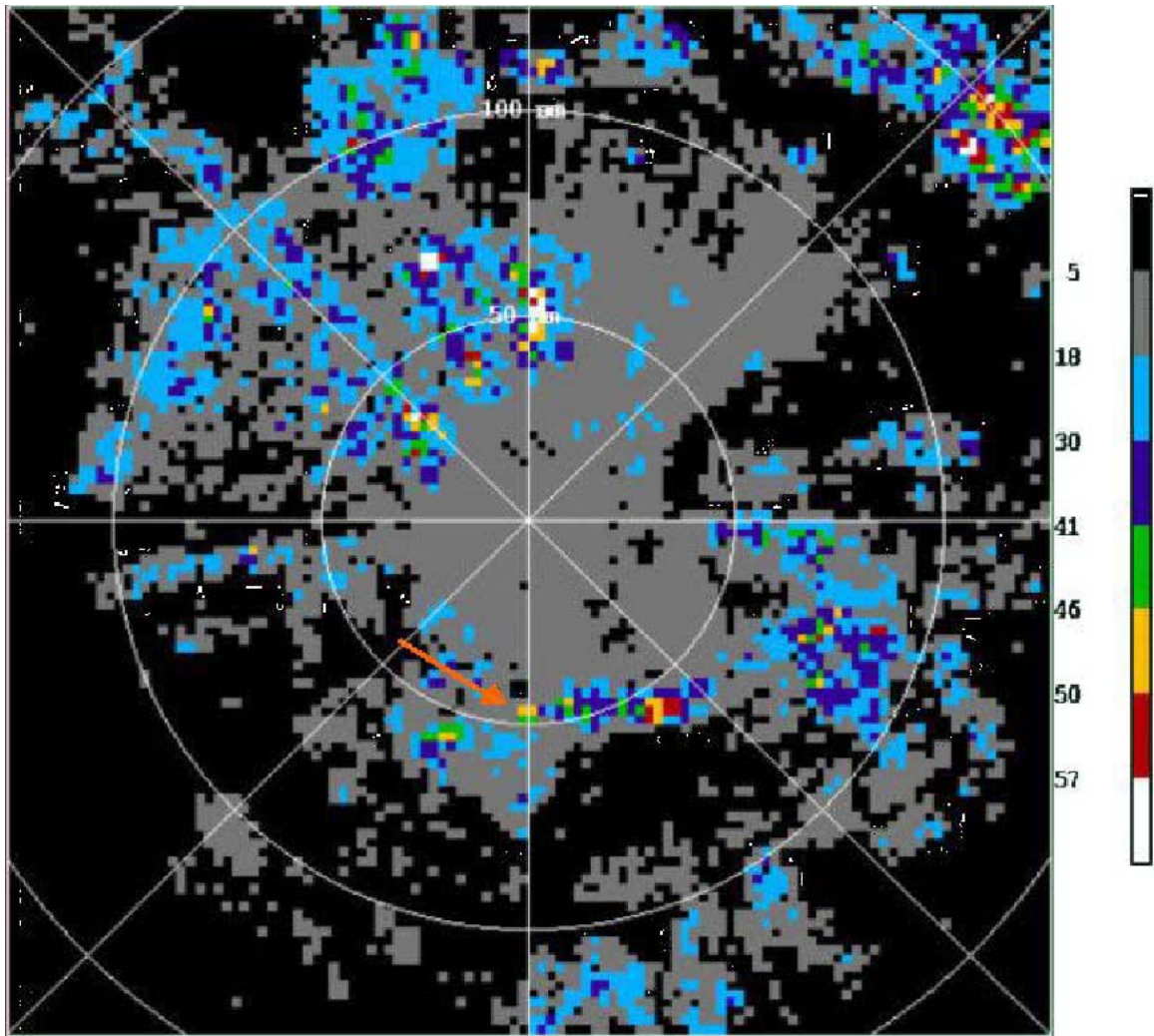


Figure 25. Composite Reflectivity without AP mitigation (ORPG product 36) for WSR-88D KFWS on July 13, 1995 at 1338 UTC. Orange arrow denotes line of convective cells with reflectivity returns near 50 dBZ.

e) Activity Schedule Changes

None.

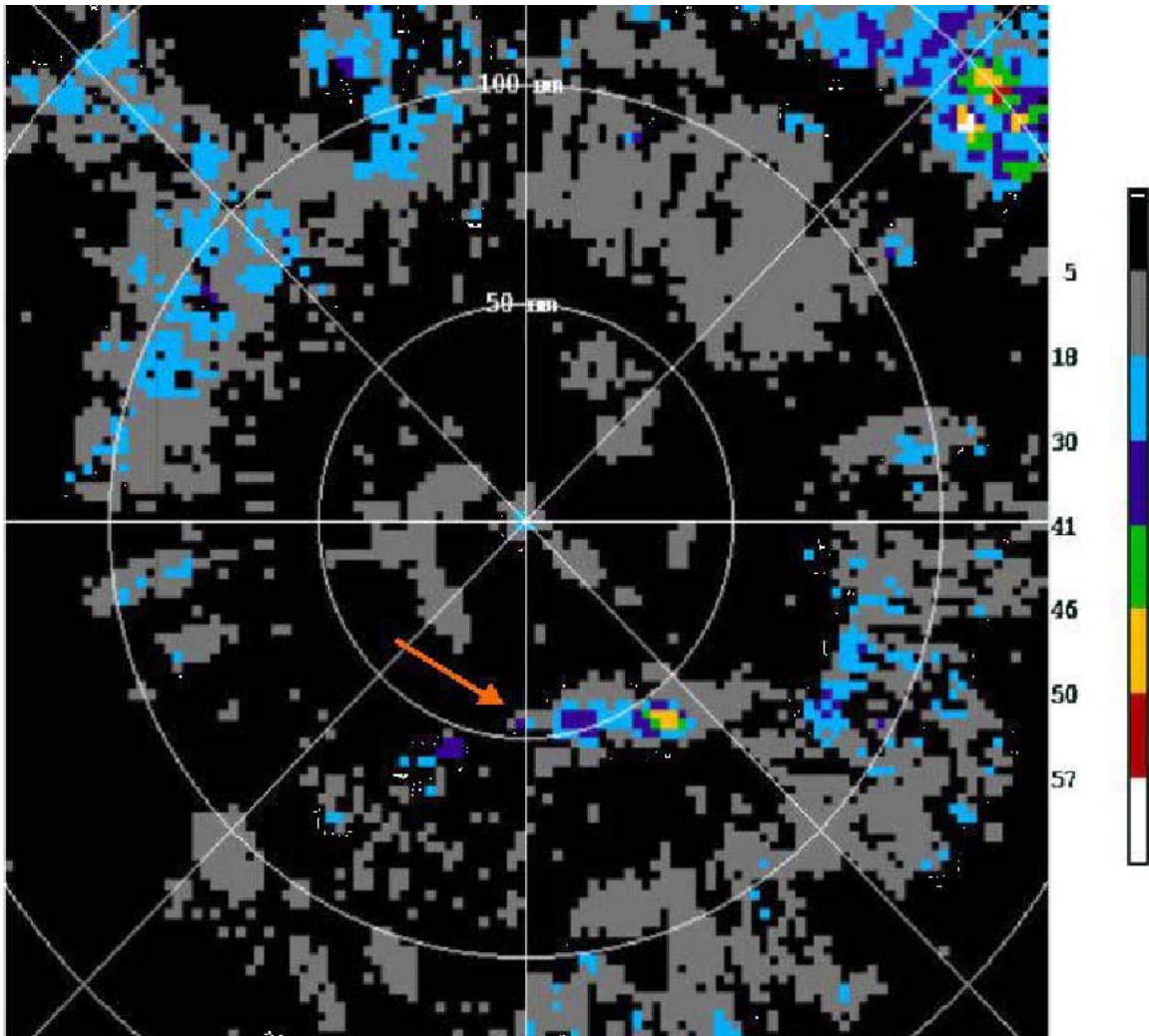


Figure 26. Same as Fig. 24 except for ORPG product 96 which includes the AP removed scheme. Some 50 dBZ reflectivity returns have been reduced to 30 dBZ or below.